2019-01-0601 Published 02 Apr 2019

Efficient Power Electronic Inverter Control Developed in an Automotive Hardware-in-the-Loop Setup

Konstantin Etzold, Claas Kürten, Andreas Thul, Lukas Müller, René Scheer, Max-Arno Meyer, Christian Granrath, Michael Schröder, Kay Hameyer, and Jakob Andert RWTH Aachen University

Citation: Etzold, K., Kürten, C., Thul, A., Müller, L. et al., "Efficient Power Electronic Inverter Control Developed in an Automotive Hardware-in-the-Loop Setup," SAE Technical Paper 2019-01-0601, 2019, doi:10.4271/2019-01-0601.

Abstract

Hardware-in-the-Loop is a common and established testing method for automotive developments in order to study interactions between different vehicle components during early development phases. Hardware-in-the-Loop setups have successfully been utilized within several development programs for conventional and electrified powertrains already. However, there is a particular shortage of studies focusing on the development of inverter controls utilizing Hardware-in-the-Loop tests. This contribution shall provide a first step toward closing this gap. In this article, inverter controls with different pulse width modulations for varying modulation index are studied at a Hardware-in-the-Loop setup. Thereto, the inverter control for an interior permanent magnet synchronous machine is developed utilizing space vector pulse width modulation with overmodulation. The starting point for the inverter control implementation includes power and loss analyses for the power electronic inverter as well as for the interior permanent magnet synchronous machine at a laboratory test bench. Comparing space vector pulse width modulation with and without overmodulation, it is determined that the system losses are reduced by 9 % and the power is increased by 8 %, which verifies the performance improvement by applying overmodulation. In addition, a real-time vehicle dynamics simulation of a battery operated electric powertrain is developed. The required driving resistance parameters for the vehicle dynamics simulation are verified based on defined vehicle coast down test results. The vehicle dynamics simulation is combined with the inverter control and the test bench components to a Hardware-in-the-Loop setup complying with real-time conditions. The power of the interior permanent magnet synchronous machine is increased by virtual scaling of its active length, which demonstrates the testing variability of the Hardware-in-the-Loop setup. This modified electric powertrain and the newly developed inverter control are tested in the class 3 worldwide harmonized light vehicles test cycle. The interactions between the inverter control and the electric powertrain are analyzed and the results are discussed. Moreover, the Hardware-in-the-Loop methodology's ability to accelerate the development process for automotive applications is demonstrated.

I. Introduction

The investments in time and costs for automotive development programs of new electric powertrains are required to decrease continuously [1, 2, 3, 4, 5, 6]. Automotive development programs usually follow the so called V-Cycle with particular periods for system specification and implementation, system integration as well as system tests and validation, see also Figure 1. During the development program, the system is specified and implemented from a macroscopic to a microscopic level increasing the depth of detail over time. Originally, the specification and implementation process is sequentially followed by the integration and thereafter, by the testing and validation processes. However, these three processes can be parallelized by rescheduling testing and validation tasks to earlier program phases. This approach is usually referred to as frontloading [1, 7]. Applying frontloading, potential errors can be detected and appropriate design changes can be applied in earlier program phases. Hence, development investments for error fixing and design changes can be reduced [1, 2, 3, 4, 5, 6].

For frontloading, Hardware-in-the-Loop (HiL) is an established testing and validation approach. Applying HiL testing, the device under test is coupled to a real-time simulation of the remaining system in order to simulate the effects of the device under test on the remaining system and vice versa. Thus, instead of testing the device under test isolated from the remaining system, the interactions between system components can be investigated at a HiL setup [10].

For electric powertrains, HiL tests can be distinguished between signal, electric and mechanical levels [11, 12, 13]. On the signal level, only the control unit is investigated as a physical component in combination with a real-time simulation [14]. In addition to the control unit, the power electronics are tested as real components on the electric level [15, 16]. On the mechanical level, the electric traction machine is added to the control unit and power electronics at the test bench,

FIGURE 1 Reduction of development investments by frontloading during the development V-Cycle, modified from [8, 9].

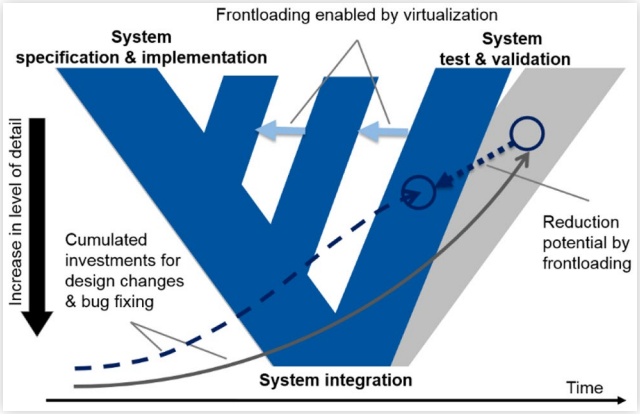

while the remaining system is simulated by the real-time simulation. In this article, an inverter control algorithm is investigated at a HiL setup on the mechanical level. HiL tests have successfully been performed on the mechanical level for conventional powertrains [10, 17, 18, 19] as well as for electrified powertrains [13, 15, 20, 21, 22, 23, 24, 25, 26]. For instance in [25], different energy storage systems of a parallel hybrid powertrain have been studied. Another contribution focused on torque vectoring of a battery electric vehicle (BEV), where the interactions between an induction machine and the simulated vehicle dynamic behavior were investigated [24]. In [13], a HiL setup was applied to an electrified hydraulic system of a working vehicle. However, there is a particular shortage of studies that consider mechanical HiL setups in order to study inverter controls with different modulations. This contribution shall provide a first step toward closing this gap in order to demonstrate how HiL setups can provide a testing scenario for the seamless development of inverter controls in a vehicular environment.

In this article, an inverter control including a space vector pulse width modulation with overmodulation is developed and tested in a HiL setup. Thereto, the real-time vehicle simulation, the inverter control and the test bench setup with virtual scaling of the active length of the IPMSM are described in chapter II. In addition, performance analyses of the IPMSM are conducted at a laboratory test bench in order to verify a power increase of 8 % and a system loss reduction of 9 % by the operation of space vector pulse width modulation with overmodulation (SVPWM-OM) compared to the operation of space vector pulse width modulation without overmodulation (SVPWM). As electric traction machine, an interior permanent magnet synchronous machine (IPMSM) has been chosen. The test bench is combined with a real-time simulation of a BEV to a HiL setup utilizing virtual scaling of the active length of the IPMSM, which demonstrates the test variability of the HiL setup. In chapter III, the class 3 worldwide harmonized light vehicles test cycle (WLTC) is conducted and the results of the inverter control with SVPWM for varying modulation index during dynamic operation are analyzed. Thereafter, the conclusions are presented in chapter IV.

II. Method - Hardware-in-the-Loop Setup Approach

A schematic of the most relevant components of the test bench setup is shown in Figure 2. In the upper area of Figure 2 is the DC source for the power supply of the test bench. The DC source is connected to the power electronics of the load machine as well as the power electronic inverter of the IPMSM. The inverter of the IPMSM is controlled by the processor which includes the inverter control and the real time vehicle simulation.

Real-Time Vehicle Simulation

The proposed vehicle simulation for the HiL setup consists of a longitudinal vehicle dynamics simulation including virtual scaling, a driver model as well as a powertrain control unit (PCU).

Vehicle Dynamics Simulation In this contribution, a battery electric vehicle (BEV) is investigated. The vehicle parameters are listed in Table 1 and describe an A segment BEV containing a traction battery with a system DC voltage of 200 V, an inverter and an interior permanent magnet synchronous machine (IPMSM). The IPMSM consists of four pole pairs and delivers a maximum torque of 250 Nm and a maximum mechanical power of 30 kW. The IPMSM is connected to the wheels by a fixed gear set and a final drive.

Similar to [27], a simplified vehicle model is considered. With the assumption of an ideal wheel behavior without slip, the longitudinal vehicle dynamics equation yields to:

$$m\frac{dv_{\mathrm{act}}}{dt} = F_{\mathrm{a}} - F_{\mathrm{d}} - F_{\mathrm{r}} - F_{\mathrm{g}}. \tag{1}$$

The effective vehicle mass m includes the inertia of the rotating powertrain components. Using the vehicle parameters from Table 1 in addition to the density of the air, as well as the road grade, the air drag force F_{d}, the rolling resistance force F_{r}, and the gravity force F_{g} are determined. F_{a} is the accelerating force at the vehicle's center of gravity. It is

FIGURE 2 Hardware-in-the-Loop setup with test bench components and processor for inverter control and vehicle simulation.

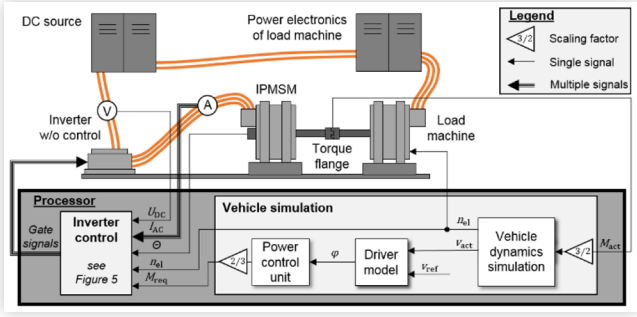

TABLE 1 Overview of relevant vehicle parameters.

	Parameter	Value	
General vehicle data	Effective vehicle weight	1310	kg
	Drag coefficient	0.43	-
	Vehicle cross-section area	2.25	m^2
	Rolling friction coefficient	0.01	-
	Wheel radius	0.295	m
Battery electric powertrain	Total gear ratio	1.95	-
	Maximum torque of IPMSM	250	Nm
	Maximum power of IPMSM	30	kW
	System voltage (OCV)	200	V

calculated with the IPMSM torque M_{act}, the friction brake torque M_{frict}, the wheel radius r_w and the total gear ratio i_{total}:

$$F_a = \frac{M_{act} \cdot i_{total}}{r_w} + \frac{M_{frict}}{r_w}. \quad (2)$$

For this HiL setup, the IPMSM torque is measured by the torque flange at the test bench and is utilized as input for the vehicle dynamics simulation illustrated in Figure 2. However, since the maximum power of the IPMSM is physically not sufficient to accelerate the vehicle according to the WLTC reference velocity, the measured torque is multiplied by a virtual scaling factor of 1.5. Applying virtual scaling, the active length of the IPMSM is assumed to be 1.5 times longer than the active length of the original IPMSM at the test bench, which leads to a virtual increase of the IPMSM torque. This demonstrates the testing variability of the HiL setup. Thus, applying virtual scaling, HiL tests can provide further perceptions about the vehicle performance with different motorizations.

The output of the vehicle dynamics simulation is the set point of the IPMSM speed n_{el}, which is transmitted to the inverter control and the load machine of the test bench. The IPMSM speed is based on the actual vehicle velocity v_{act} which is obtained from integration of equation (1).

Driver Model The actual vehicle velocity v_{act} and the reference velocity v_{ref} of the WLTC are the inputs of the driver model. A proportional integral (PI) control driver model with anti-windup strategy is applied here [28]. The driver model minimizes the difference between reference and actual vehicle velocity by setting the driver command value φ. The driver command value ranges between −1 and 1, where negative values imply desired braking, and positive values acceleration. The driver command value is sent to the PCU.

Powertrain Control Unit The PCU interprets the driver command and sets appropriate torque command values. In case of a braking scenario, the driver command value is negative, and the PCU linearly scales the maximum braking torque with the negative driver command value. A 100-percent friction braking strategy is implemented, meaning all braking force is applied with the friction brakes of the vehicle. Consequently, no regenerative braking is utilized, which is subject to future work at this HiL setup. In acceleration cases, the positive driver command values are multiplied with the speed dependent maximum IPMSM torque in order to obtain the requested IPMSM torque M_{req}.

Verification of the Vehicle Simulation

For the verification, the driving resistances of the vehicle dynamics simulation and the controller settings of the driver model are evaluated.

Verification of the Driving Resistances The proposed vehicle model is validated by performing coast down tests, both in simulation and real world experiments. The coast down measurements are conducted with a vehicle of the same model series similar to the simulated BEV. At an ambient temperature of 15 °C, the tests are performed on a flat outdoor coast down track, which is protected from wind influences. For each test, the vehicle is accelerated to a velocity of 128 km/h. After reaching this velocity, the IPMSM torque is set to zero. Air drag resistance, as well as rolling resistances decelerate the vehicle. Multiple measurements are performed in both driving directions and the arithmetic means are calculated for each direction. Figure 3 shows the comparison between the measured mean values compared to the simulated BEV. The differences between the two driving directions can be due to marginally different wind conditions and possible grade influences. The curve for the simulated vehicle is within the area of measured coast down characteristics. This proves sufficient accuracy.

Verification of the Driver Model The driver model is calibrated and validated with a Model-in-the-Loop (MiL) simulation according to the WLTC regulations. The velocity profile is depicted in Figure 4. A maximum velocity difference between reference velocity and simulated speed of 1.8 km/h is determined, which is within the permissible velocity tolerance of the WLTC regulations [29]. This confirms the appropriate settings of the driver model.

Inverter Control

For this HiL test, an inverter control with space vector modulation (SVPWM) is developed. In case that the DC voltage U_{DC} limits the IPMSM operation, overmodulation

FIGURE 3 Coast down characteristics of the simulated BEV and mean values of the measured experiments of an A segment vehicle in both directions of the test track.

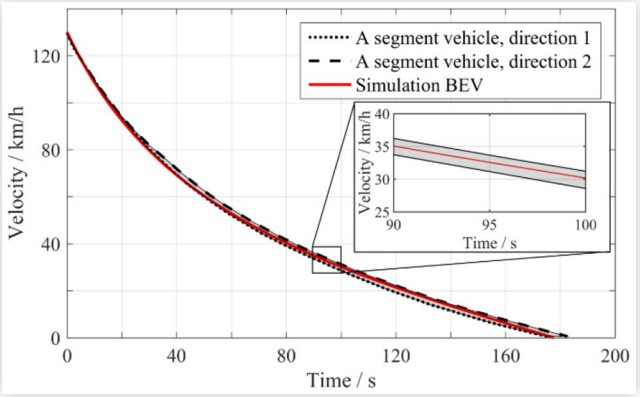

FIGURE 4 Simulated vehicle velocity and velocity difference during the WLTC.

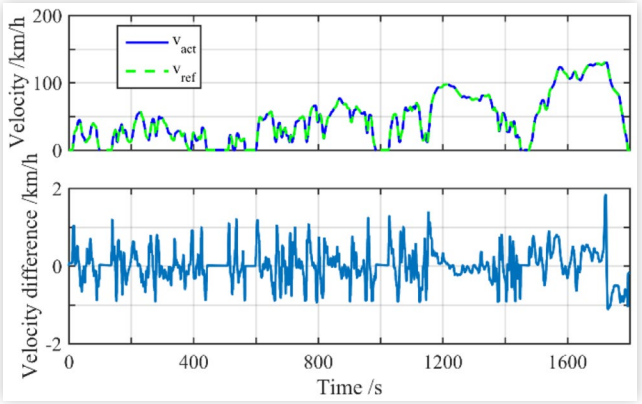

(SVPWM-OM) is applied in order to increase the DC voltage utilization. The detailed functions of the inverter control are described in the following sections.

The interconnections between the inverter control and the remaining HiL setup are illustrated in Figure 2, there are multiple input signals going to the inverter control block. The requested torque M_{req} is provided by the PCU and it is virtually scaled by a factor of 1.5. In addition to the requested torque, the measured signals of the AC currents I_{AC}, DC voltage U_{DC} and the rotor angle θ of the IPMSM are further input quantities. The gate signals of the inverter control are sent to the inverter to set the requested I_d and I_q currents according to the requested torque. The detailed sections of the inverter control are illustrated in Figure 5. These sections include lookup tables (LUT), current control, flux linkage control, voltage limitation and SVPWM.

Lookup Tables The LUT are based on finite element method (FEM) simulations of the IPMSM. The requested torque and the current flux linkage are the input quantities. According to these input quantities, the requested currents $I_{d,req}$ and $I_{q,req}$ are determined considering maximum torque per ampere (MTPA) for operation points within the base speed. For operation points larger than the base speed, field weakening and maximum torque per flux linkage (MTPF) are utilized [30]. Applying these principles, the currents I_d and I_q are optimized with respect to a minimum magnitude of the entire current vector in order to reduce copper and iron losses at the IPMSM as well as conduction losses at the inverter.

Current Control Besides the requested currents $I_{d,req}$ and $I_{q,req}$, the measured DC voltage U_{DC}, the rotor angle θ as well as the AC currents I_{AC} are further inputs for the current control. The measured AC currents are transformed into the actual currents I_d and I_q, considering the Clarke Park transformation [31]. Based on the differences between requested and actual currents, the requested voltages $U_{d,req}$ and $U_{q,req}$ are determined by PI controllers. In addition to the PI current controllers, feed forward controls adjust the requested voltages $U_{d,req}$ and $U_{q,req}$ with respect to the flux linkages Ψ_d and Ψ_q as well as the electrical rotational speed.

Flux Linkage Control The input signals of the flux control are the requested voltages $U_{d,req}$, $U_{q,req}$ and U_{DC} as well as the electrical rotational speed n_{el}. Considering these quantities, the flux linkage Ψ yields to:

$$\Psi = \frac{\sqrt{U_{d,req}^2 + U_{q,req}^2}}{2 \cdot \pi \cdot n_{el}} < \frac{U_{lim}}{2 \cdot \pi \cdot n_{el}}. \quad (3)$$

The flux linkage is controlled by a PI controller adhering to the voltage limit U_{lim} and the electrical rotational speed n_{el}. For SVPWM, the theoretical voltage limit is 57.7 % of the DC voltage [32]. This voltage limit $U_{max,stat}$ is selected for stationary operation points. By applying space vector pulse width modulation with overmodulation (SVPWM-OM), the theoretical voltage limit can be increased up to 60.6 % of the DC voltage [33]. In Figure 8, this voltage limit $U_{max,tran}$ can be illustrated by utilizing the entire voltage hexagon in α-β-coordinates. The voltage limit $U_{max,tran}$ is utilized for transient operation. Thus, by utilizing a higher voltage limit for transient operation compared to $U_{max,stat}$ for stationary operation, a voltage reserve is provided in order to ensure a quick response to a current request.

The controlled flux linkage is the input of the LUT. The functionality and the interactions of the flux linkage control, the LUT and the current control can be described in the I_d-I_q-plane of Figure 6. Based on a constant torque request and

FIGURE 5 Inverter control with flux linkage control and voltage limitation for space vector pulse width modulation with overmodulation (SVPWM-OM).

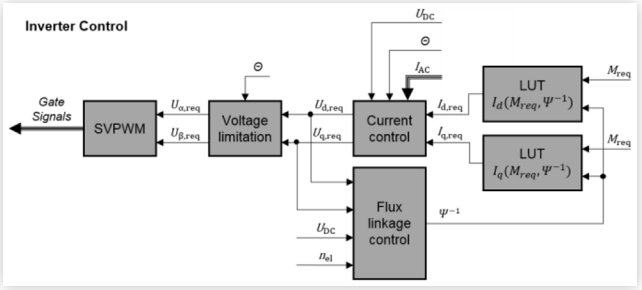

FIGURE 6 Principle operation of the interactions between flux linkage control and LUT in the I_d-I_q-plane.

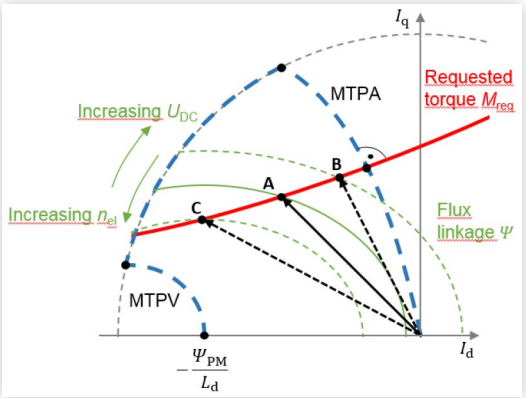

a defined flux linkage, the requested current vector is provided (point A). If the DC voltage increases or the IPMSM speed decreases, the flux linkage increases. Thus, the current vector is shifted toward the MTPA curve (point B), which leads to a higher efficiency due to a shorter current vector magnitude. However, if the flux linkage decreases due to a higher speed or lower DC voltage, the current vector is shifted toward negative d-axis (point C). Thus, the flux linkage control operates only during field weakening operation.

Voltage Limitation for Space Vector Pulse Width Modulation with Overmodulation For SVPWM-OM, the voltage limit varies as a function of the rotor position. Since this is not considered in the flux linkage control, the section voltage limitation is implemented, see also Figure 5. In the literature, there are multiple voltage limitation approaches. Common approaches are voltage limitation with minimum phase error or with preference of the current I_d or limitation of the dynamic part of the voltage space vector [34, 35]. For this contribution, the linear voltage limitation has been chosen because of its simplicity and its robust control when compared to the other approaches. For linear voltage limitation, the requested voltages $U_{d,req}$ and $U_{q,req}$ are transformed into the voltages $U_{\alpha,req}$ and $U_{\beta,req}$ of the α-β-coordinates system, applying the inverse Park transformation [31]. If the requested voltage vector exceeds the voltage limit $U_{max,tran}$ illustrated by the hexagon in Figure 8, the requested voltage vector is limited keeping the angle constant. Thus, the length of the voltage vector varies depending on the angular position inside the hexagon.

In Figure 5, the last section of the inverter control is entitled SVPWM. In this section, the voltages $U_{\alpha,req}$ and $U_{\beta,req}$ are converted into six gate signals for the insulated gate bipolar transistors (IGBT) of the inverter. For this conversion, space vector pulse width modulation is applied [36].

Verification of the Inverter Control at the Test Bench

The inverter control is verified at the test bench by power and loss analyses for motoring operation. The test results are analyzed regarding the question if the implemented inverter control with SVPWM-OM leads to an increase of system power and a decrease of system losses. In addition, SVPWM-OM is studied in terms of utilizing the full voltage range up to the voltage limit $U_{max,tran}$.

Power and Loss Analyses of the Performance Tests For the performance tests, the DC voltage is set to 200 V and the cooling temperature of the conditioning system is 21 °C. The tests start with a conditioning phase during which the IPMSM is operated at 1000 rpm and 140 Nm until a stator temperature of 64 °C is reached. Within 2 s, speed and torque are ramped to the measurement point and stabilized. The actual measurement is taken for 3 s. For the following measurement point, the IPMSM is conditioned again.

The first test is performed with SVPWM for all operation points. For the second test, the inverter control operates SVPWM for the operation points which are not limited by the DC voltage. If the DC voltage limit is reached, the inverter control applies SVPWM-OM for the second test in order to increase the voltage utilization. For both tests, the losses of the entire system are analyzed and compared. In Figure 7, the loss differences for the inverter and IPMSM are presented. During low speed and low torque, both inverter controls have similar losses. However, for increasing torque and speed, the loss differences are negative, which means that the SVPWM-OM leads to lower losses. The system losses can be reduced by 9 % at 1500 rpm and 190 Nm. These reduced losses are due to smaller current as well as iron losses. These losses are smaller due to smaller currents by applying a higher voltage utilization. This confirms the principle of the implemented flux linkage control with a higher voltage utilization during field weakening operation with SVPWM-OM.

FIGURE 7 Measured loss differences comparing SVPWM with SVPWM-OM at a DC voltage of 200 V and an IPMSM temperature of 64 °C.

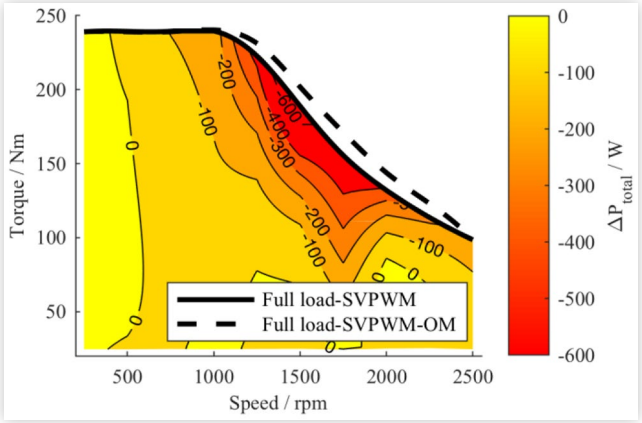

Furthermore, the full load curves for SVPWM and SVPWM-OM are presented. Both modulations yield almost the same maximum torque during base speed operation. However, the SVPWM-OM provides a larger maximum torque for higher speeds, which consequently leads to higher power. Applying SVPWM-OM, the maximum power can be increased by up to 8 % when compared to the maximum power of SVPWM. In summary, these test results verify a higher efficiency and a higher available power by applying SVPWM-OM, which confirms that this is a plausible implementation of the inverter control.

Overmodulation during the Performance Tests The higher DC voltage utilization due to the SVPWM-OM implementation is demonstrated in Figure 8 for an operation point of 1500 rpm and 150 Nm. The measurement was taken for 3 s at a sample rate of 10 kHz. The requested voltage vectors of $U_{\alpha,req}$ and $U_{\beta,req}$ are marked as brown marks $U_{\alpha-\beta,req}$. The majority of the requested voltages $U_{\alpha-\beta,req}$ are inside the circular voltage limit $U_{max,stat}$. However, some requested voltages $U_{\alpha-\beta,req}$ exceed the voltage limit $U_{max,stat}$ illustrated by the hexagon. These voltages are marked green as $U_{\alpha-\beta,lim}$. Further, they confirm that overmodulation is applied, which enables utilizing the voltage reserves in the corner of the hexagon. All voltages $U_{\alpha-\beta,lim}$ stay within the hexagon, even though there are requested voltages $U_{\alpha-\beta,req}$

FIGURE 8 Measured voltage vectors for SVPWM-OM in α-β-coordinates for 1500 rpm and 150 Nm.

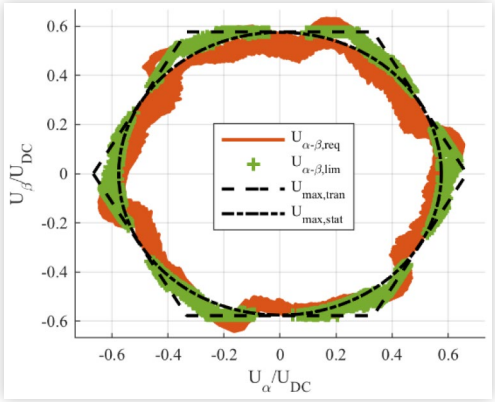

outside the hexagon, e.g. −0.45 U_α/U_{DC} and 0.47 U_β/U_{DC}. This proves the proper operation of the voltage limitation by reducing the requested voltages $U_{\alpha-\beta,req}$ outside the hexagon and setting new values $U_{\alpha-\beta,lim}$ inside the hexagon.

III. Results and Discussion

In this contribution, the interactions between inverter control with SVPWM-OM and the vehicle dynamic behavior are analyzed at the HiL setup.

Evaluation of Vehicle Velocity during the WLTC

On top of Figure 9, the vehicle velocity profile v_{act} is depicted over time for the worldwide harmonized light vehicle testing cycle (WLTC). This velocity is based on the measured IPMSM speed at the test bench. For this HiL setup, the IPMSM speed is mainly effected by the controller settings of the driver model, the PCU, the inverter control and the load machine control. The settings for the driver model and the PCU had already been aligned in the MiL setup before, see also Figure 4. A comparison of the reference velocity and the actual vehicle velocity indicates the proper alignment of the controllers. In Figure 9, the actual vehicle velocity v_{act} shows a favorable congruence to the WLTC reference velocity v_{ref}. The velocity differences between reference and actual velocity are illustrated underneath. With a maximum velocity difference of 1.9 km/h at 667 s, the velocity difference is within the permissible velocity tolerance of 2 km/h as required by the WLTC regulations [29]. Thus, for this HiL setup, the controller settings of the driver model, PCU, inverter control and load machine control are accurately aligned.

FIGURE 9 Hardware-in-the-Loop measurements of the velocity profile and energy demand during the WLTC with indication for SVPWM-OM.

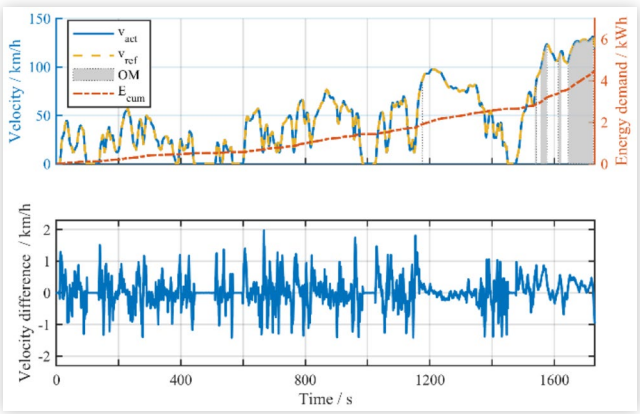

Evaluation of the Inverter Control during Dynamic Operation

For the majority of the IPMSM operation during the WLTC, the DC voltage is sufficient. Hence, the inverter control is operated with SVPWM. However, at 1175 s and during the extra high velocity section from 1538 s onwards, SVPWM-OM is occasionally applied. SVPWM-OM is detected when the flux linkage Ψ based on the speed and DC voltage measurements exceeds the flux linkage threshold which is based on $U_{max,stat}$ according to equation (3). However, the measurements were taken at a sample rate of 200 Hz. Since this is significantly slower than the inverter sample rate of 10 kHz, some sections of SVPWM-OM might be missing and further measurements with higher sample rates should be conducted in the future. The operations with SVPWM-OM are marked by a gray area in Figure 9. Especially during acceleration, the inverter control switches from SVPWM to SVPWM-OM. During these accelerations, the IPMSM speed is already high, which leads to a reduced flux linkage. In addition, high torque values and therefore, high currents are requested so that the flux linkage threshold is exceeded and SVPWM-OM is applied.

For the WLTC, the I_d and I_q currents are measured and illustrated in Figure 10 and Figure 11. The I_q currents are positive during the entire test cycle, which indicates motoring operation. The negative values of the I_d currents present the usual operation of the IPMSM. Furthermore, the current differences between set values and measured values are depicted in addition to the orange indicator for SVPWM-OM. The current differences are positive as well as negative which can be interpreted as current ripples or oscillations of the measured current values around the current set values. From the beginning until 990 s, the low and medium velocity sections of the WLTC are tested. During this period, the current differences for I_d and I_q oscillate with amplitudes from almost 1 A during stand still, e.g. for ΔI_d at 580 s, to 4 A during driving operation, e.g. for ΔI_d at 961 s. The oscillating current difference is steady and no significant peaks are determined even for high current amplitudes. Therefore, there is no significant dependency of the current oscillations on the current amplitude for this HiL test. When SVPWM-OM is determined, the current difference increases significantly, e.g. the maximum current difference ΔI_d is almost 16 A at 1543 s and the maximum current difference ΔI_q is 10 A. These current differences can be caused by the variation of the voltage vector

FIGURE 10 Differences between measured $I_{q,act}$ current and ΔI_q current difference between measured and set values during WLTC.

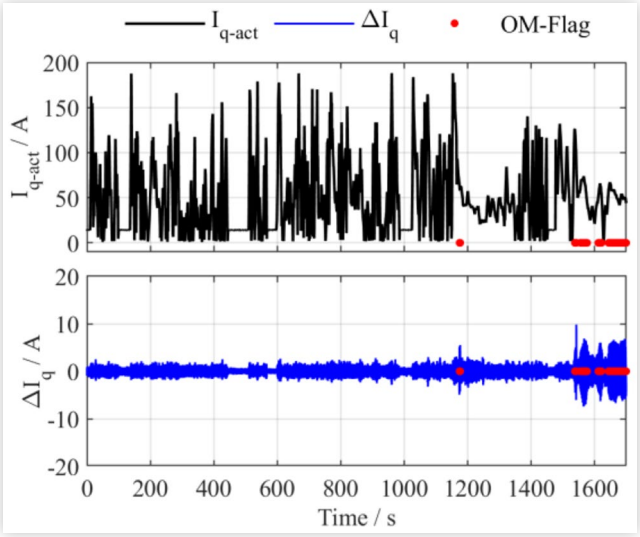

FIGURE 11 Differences between measured $I_{d,act}$ current and ΔI_d current difference between measured and set values during WLTC.

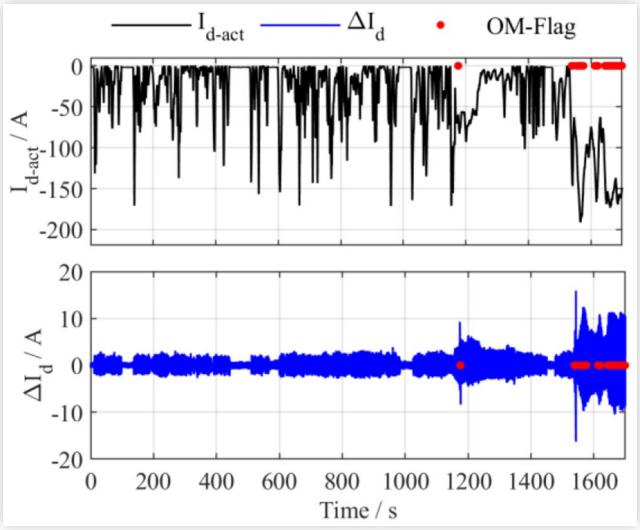

oscillation during SVPWM-OM. These voltage vector oscillations are due to the volatile voltage limit, which effects the current control.

The current oscillations can have negative impacts on the torque and the efficiency as well as the acoustic behavior of the IPMSM. Therefore, these impacts should be further investigated in the future and the current oscillations should be reduced. The reduction of the current oscillations can be achieved by further calibrations of the current control. For calibration tasks, this HiL setup provides a favorable testing scenario since it considers interdependencies between the inverter control and the vehicle dynamics behavior. Hence, adjustments of the inverter control can directly be implemented and tested at a laboratory test bench and the effects on the driving behavior during the WLTC can be studied within a comprehensive vehicular environment.

IV. Conclusions

In this article, the feasibility of an automotive HiL setup is proven for testing and validation of inverter controls with different SVPWM for varying modulation index. Thereto, a vehicle simulation of a BEV was designed and verified at a MiL setup. Furthermore, the inverter control with SVPWM and SVPWM-OM was developed. Performance tests of the IPMSM and the inverter were conducted at a laboratory test bench and the test results were compared for both inverter control modulations. Applying SVPWM-OM, a higher voltage utilization was determined. This led to a reduction of system losses by 9 % and an increase of power by up to 8 %, which confirm a plausible implementation of the SVPWM-OM. Finally, the real-time vehicle simulation, the test bench and the inverter control with SVPWM-OM were combined to a HiL setup utilizing virtual scaling of the active length of the IPMSM. Applying virtual scaling, the testing variability of the HiL setup was demonstrated. The controller settings were aligned so that the simulated vehicle velocity as well as the resultant IPMSM speed at the test bench could follow the reference velocity very well. The WLTC was performed and the different inverter control modulations and their timing during the WLTC were identified. During operation of SVPWM-OM, the test results show a significant increase of the current ripple which should be reduced by further calibrations at the HiL setup. This indicates the relevance of HiL setups for studies of the interactions between inverter controls, electric powertrains and vehicle dynamics in early development phases and represents a further example how HiL testing can support frontloading for automotive development programs.

References

1. Kerga, E., Schmid, R., Rebentisch, E., and Terzi, S., "Modeling the Benefits of Frontloading and Knowledge Reuse in Lean Product Development," in *2016 Portland International Conference on Management of Engineering and Technology (PICMET)*, Honolulu, USA, 04.09.2016 - 08.09.2016, IEEE, 2532-2542.
2. Andert, J., Klein, S., Savelsberg, R., Pischinger, S. et al., "Virtual Shaft: Synchronized Motion Control for Real Time Testing of Automotive Powertrains," *Control Engineering Practice* 56:101-110, 2016, doi:10.1016/j.conengprac.2016.08.005.
3. Xia, F., Lee, S.-Y., Andert, J., Kampmeier, A. et al., "Crank-Angle Resolved Real-Time Engine Modelling A Seamless Transfer from Concept Design to HiL Testing," SAE Technical Paper 2018-01-1245, 2018, doi:10.4271/2018-01-1245.
4. Schiffbaenker, P. and Shankavaram, R., "Following the Path to Electrification with a Holistic Battery Development Approach," in *2017 IEEE Transportation Electrification*

Conference (ITEC-India), Pune, 13.12.2017-15.12.2017, IEEE, 2017, 1-6, ISBN 978-1-5386-2668-9.

5. Eisenbarth, M., Etzold, K., Andert, J., Plum, T. et al., "A Holistic Methodology for the Development of Connected Hybrid Vehicles," in *Symposium für Entwicklungsmethodik 2017*, 2017.
6. Etzold, K., Granrath, C., Klein, S., Eisenbarth, M. et al., "Virtuelle Elektrifizierung - Ein nahtloser Entwicklungsprozess für Closed-Loop-Testing von elektrischen Antriebsstraengen," in *E-MOTIVE Expertenforum*, Hannover, Germany, 2017.
7. Thomke, S., "The Effect of "Front-Loading" Problem-Solving on Product Development Performance," *Journal of Product Innovation Management* 17(2):128-142, 2000, doi:10.1016/S0737-6782(99)00031-4.
8. Muli, M. and Cassar, J., "Virtual Validation-A New Paradigm in Controls Engineering," SAE Technical Paper 2013-01-2404, 2013, doi:10.4271/2013-01-2404.
9. Schäuffele, J. and Zurawka, T., "Automotive Software Engineering: Grundlagen, Prozesse, Methoden und Werkzeuge," . In: *ATZ/MTZ-Fachbuch*. 2nd Edition. (Wiesbaden, Vieweg+Teubner Verlag, 2004). ISBN:978-3-322-91947-2.
10. Fathy, H.K., Filipi, Z.S., Hagena, J., and Stein, J.L., "Review of Hardware-in-the-Loop Simulation and Its Prospects in the Automotive Area," in *Modeling and Simulation for Military Applications; Proceedings Volume 6228, Defense and Security Symposium*, Orlando (Kissimmee), United States, 2006.
11. Wagener, A., Schulte, T., Waeltermann, P., and Schuette, H., "Hardware-in-the-Loop Test Systems for Electric Motors in Advanced Powertrain Applications," SAE Technical Paper 2007-01-0498, 2007, doi:10.4271/2007-01-0498.
12. Bouscayrol, A., "Different Types of Hardware-In-the-Loop Simulation for Electric Drives," *2008 IEEE International Symposium on Industrial Electronics*, Cambridge, 30.06.2008-02.07.2008, IEEE, 2008, 2146-2151, ISBN 978-1-4244-1665-3.
13. Mocera, F. and Soma, A., "Study of a Hardware-In-the-Loop Bench for Hybrid Electric Working Vehicles Simulation," in *2017 Twelfth International Conference on Ecological Vehicles and Renewable Energies (EVER)*, Monte-Carlo, Monaco, 11.04.2017-13.04.2017, IEEE, 1-8, ISBN 978-1-5386-1692-5.
14. Li, W., Gregoire, L.-A., Souvanlasy, S., and Belanger, J., "An FPGA-Based Real-Time Simulator for HIL Testing of Modular Multilevel Converter Controller," *IEEE Energy Conversion Congress and Exposition (ECCE) 2014*, Pittsburgh, USA, 9/14/2014-9/18/2014, IEEE, 2088-2094, ISBN 978-1-4799-5776-7.
15. Lemaire, M., Sicard, P., and Belanger, J., "Prototyping and Testing Power Electronics Systems Using Controller Hardware-In-the-Loop (HIL) and Power Hardware-In-the-Loop (PHIL) Simulations," in *2015 IEEE Vehicle Power and Propulsion Conference (VPPC)*, Montreal, Canada, 10/19/2015-10/22/2015, IEEE, 1-6, ISBN 978-1-4673-7637-2.
16. Zyuzev, A.M., Mudrov, M.V., and Nesterov, K.E., "PHIL-System for Electric Drives Application," in *2016 IX International Conference on Power Drives Systems (ICPDS)*, Perm, Russia, 3-7.10.2016, IEEE, 1-4, ISBN 978-1-5090-1474-3.
17. Guse, D., Klein, S., Andert, J., Pischinger, S. et al., "Virtual Transmission Evaluation Using an Engine-in-the-Loop Test Facility," SAE Technical Paper 2018-01-1361, 2018, doi:10.4271/2018-01-1361.
18. Klein, S., Griefnow, P., Guse, D., Xia, F. et al., "Virtual 48V Mild Hybridization: Efficient Validation by Engine-in-the-Loop," *SAE Int. J. Alt. Power.* 7(3), 2018, doi:10.4271/2018-01-0410.
19. Klein, S., Savelsberg, R., Xia, F., Guse, D. et al., "Engine in the Loop: Closed Loop Test Bench Control with Real-Time Simulation," *SAE Int. J. Commer. Veh.* 10(1):95-105, 2017, doi:10.4271/2017-01-0219.
20. Schupbach, R.M. and Balda, J.C., "A Versatile Laboratory Test Bench for Developing Powertrains of Electric Vehicles," in *Proceedings IEEE 56th Vehicular Technology Conference*, Vancouver, Canada, 24-28 Sept. 2002, IEEE, 1666-1670, ISBN 0-7803-7467-3.
21. Filipi, Z., Fathy, H., Hagena, J., Knafl, A. et al., "Engine-in-the-Loop Testing for Evaluating Hybrid Propulsion Concepts and Transient Emissions - HMMWV Case Study," SAE Technical Paper 2006-01-0443, 2006, doi:10.4271/2006-01-0443.
22. Oh, S.C., "Evaluation of Motor Characteristics for Hybrid Electric Vehicles Using the Hardware-in-the-Loop Concept," *IEEE Trans. Veh. Technol.* 54(3):817-824, 2005, doi:10.1109/TVT.2005.847228.
23. Tabbache, B., Aboub, Y., Marouani, K., Kheloui, A. et al., "A Simple and Effective Hardware-in-the-Loop Simulation Platform for Urban Electric Vehicles," in *2012 First International Conference on Renewable Energies and Vehicular Technology*, Nabeul, Tunisia, 26.03.2012-28.03.2012, IEEE, 251-255, ISBN 978-1-4673-1170-0.
24. Hu, Z., "Optimization-Based Robust Control for High-Performance Torque Vectoring in Electric Vehicles Operated by Induction Traction Motors," Dissertation, RWTH Aachen University, 2017.
25. Trigui, R., Jeanneret, B., Malaquin, B., and Plasse, C., "Performance Comparison of Three Storage Systems for Mild HEVs Using PHIL Simulation," *IEEE Trans. Veh. Technol.* 58(8):3959-3969, 2009, doi:10.1109/TVT.2009.2028146.
26. Mudrov, M., Ziuzev, A., Nesterov, K., and Valtchev, S., "Asynchronous Electric Drive Power-Hardware-in-the-Loop System," in *2018 17th International Ural Conference on AC Electric Drives (ACED)*, Ekaterinburg, Russia, March 26-30, 2018, IEEE, 1-5, ISBN 978-1-5386-2422-7.
27. Wallscheid, O. and Bocker, J., "Derating of Automotive Drive Systems Using Model Predictive Control," in *2017 IEEE International Symposium on Predictive Control of Electrical Drives and Power Electronics (PRECEDE)*, Pilsen, Czech Republic, 04.09.2017-06.09.2017, IEEE, 31-36, ISBN 978-1-5386-0507-3.
28. Liu, J., "Modeling, Configuration and Control Optimization of Power-Split Hybrid Vehicles," Dissertation, University of Michigan, 2007.
29. European Parliament, "COMMISSION REGULATION (EU) 2017/1151," Rev. 2017.
30. Liu, Q. and Hameyer, K., "A Deep Field Weakening Control for the PMSM Applying a Modified Overmodulation

Strategy," in *8th IET International Conference on Power Electronics, Machines and Drives (PEMD 2016)*, Glasgow, UK, 19-21 April 2016, IEEE, 6, ISBN 978-1-78561-188-9.

31. Duesterhoeft, W.C., Schulz, M.W., and Clarke, E., "Determination of Instantaneous Currents and Voltages by Means of Alpha, Beta, and Zero Components," *Trans. Am. Inst. Electr. Eng.* 70(2):1248-1255, 1951, doi:10.1109/T-AIEE.1951.5060554.
32. Probst, U., *Leistungselektronik für Bachelors: Grundlagen und praktische Anwendungen*, 3rd ed., Carl Hanser Fachbuchverlag, s.l., 2015, ISBN 978-3-446-44428-7.
33. Gemaßmer, T., "Effiziente und dynamische Drehmomenteinprägung in hoch ausgenutzten Synchronmaschinen mit eingebetteten Magneten," Zugl.: Karlsruhe, KIT, Diss., 2015, Technische Informationsbibliothek u. Universitätsbibliothek; KIT Scientific Publishing, Hannover, Karlsruhe, ISBN 9783731503668, 2015.
34. Gemassmer, T., Richter, J., Schnarrenberger, M., and Braun, M., "Dynamic Overmodulation for Highly Dynamic Current Control of IPMSM with Saturation Characteristics," in *International Symposium on Power Electronics, Electrical Drives, Automation and Motion (SPEEDAM), 2014*, Ischia, Italy, 6/18/2014-6/20/2014, IEEE, 842-847, ISBN 978-1-4799-4749-2.
35. Lerdudomsak, S., Doki, S., and Okuma, S., "Voltage Limiter Calculation Method for Fast Torque Response of IPMSM in Overmodulation Range," in *35th Annual Conference of IEEE Industrial Electronics, 2009*, Porto, Portugal, 11/3/2009-11/5/2009, IEEE, 1383-1388, ISBN 978-1-4244-4648-3.
36. Rathnakumar, D., LakshmanaPerumal, J., and Srinivasan, T., "A New Software Implementation of Space Vector PWI," in *Proceedings of the IEEE SoutheastCon 2005*, Ft. Lauderdale, USA, April 8-10, 2005, IEEE, 131-136, ISBN 0-7803-8865-8.

Contact Information

M. Sc. Konstantin Etzold
Institute for Combustion Engines
RWTH Aachen University
Forckenbeckstr. 4
52074 Aachen, Germany
+49 241 80 24 237
etzold@vka.rwth-aachen.de

Acknowledgment

This work was funded by the Deutsche Forschungsgemeinschaft (DFG) - GRK1856.

Definitions/Abbreviations

BEV - Battery electric vehicle
HiL - Hardware-in-the-Loop
IGBT - Insulated gate bipolar transistor
IPMSM - Interior permanent magnet synchronous machine
LUT - Lookup table
MiL - Model-in-the-Loop
MTPA - Maximum torque per ampere curve
MTPF - Maximum torque per flux curve
OCV - Open circuit voltage
OM - Overmodulation
PCU - Power control unit
PI - Proportional integral
SVPWM - Space vector pulse width modulation
WLTC - Class 3 worldwide harmonized light vehicle testing cycle

ISSN 0148-7191